Atmospheric Environment 84 (2014) 222–229

Contents lists available at ScienceDirect

Atmospheric Environment

journal homepage: www.elsevier.com/locate/atmosenv

Secondary organic aerosol formation initiated from reactions between ozone and surface-sorbed squalene

Chunyi Wang, Michael S. Waring*

Drexel University, Department of Civil, Architectural and Environmental Engineering, 3141 Chestnut St., Philadelphia, PA 19104, USA

HIGHLIGHTS

- Secondary organic aerosol (SOA) from ozone/squalene surface reactions was explored.
- High ozone and air exchange chamber conditions emphasized surface reaction role.
- SOA number and mass formed appreciably for all but one experiment out of thirteen.
- This process likely increases indoor particle number concentrations more than mass.

ARTICLE INFO

Article history:
Received 12 July 2013
Received in revised form
23 October 2013
Accepted 4 November 2013

Keywords:
Indoor air chemistry
Ozone
Squalene
Fine and ultrafine particles
Aerosol mass fraction

ABSTRACT

Previous research has shown that ozone reactions on surface-sorbed D-limonene can promote gas phase secondary organic aerosol (SOA) formation indoors. In this work, we conducted 13 steady state chamber experiments to measure the SOA formation entirely initiated by ozone reactions with squalene sorbed to glass, at chamber ozone of 57–500 ppb for two relative humidity (RH) conditions of 21% and 51%, in the absence of seed particles. Squalene is a nonvolatile compound that is a component of human skin oil and prevalent on indoor surfaces and in settled dust due to desquamation. The size distributions, mass and number secondary emission rates (SER), aerosol mass fractions (AMF), and aerosol number fractions (ANF) of formed SOA were quantified. The surface AMF and ANF are defined as the change in SOA mass or number formed, respectively, per ozone mass consumed by ozone–squalene reactions. All experiments but one exhibited nucleation and mass formation. Mass formation was relatively small in magnitude and increased with ozone, most notably for the RH = 51% experiments. The surface AMF was a function of the chamber aerosol concentration, and a multi-product model was fit using the 'volatility basis set' framework. Number formation was relatively strong at low ozone and low RH conditions. Though we cannot extrapolate our results because experiments were conducted at high air exchange rates, we speculate that this process may enhance particle number more than mass concentrations indoors.

1. Introduction

People are exposed to fine particles indoors, where many spend the majority of their lives (Klepeis et al., 2001). Secondary organic aerosol (SOA) formation, which generates particles as the result of the oxidation of reactive organic gases (ROGs), may be an important indoor source. This ROG oxidation yields many products, some of which are semivolatile and form SOA, including carboxylic acids, carbonyls, hydroperoxides, and/or organic nitrates (Kroll and Seinfeld, 2008). At typical indoor reactant concentrations, SOA formation is typically due to ROG ozonolysis, and SOA can be formed via either nucleation or partitioning mechanisms. Ozone is transported from outdoors to indoors by air exchange (Weschler, 2000) and sometimes is emitted by indoor sources such as office equipment (Lee et al., 2001) or ozone or ion generators (Waring et al., 2008; Waring and Siegel, 2011). ROGs are often emitted indoors due to consumer product usage primarily as terpenoids (Nazaroff and Weschler, 2004; Singer et al., 2006). As a result, most indoor SOA formation research has focused on the ozonolysis of terpenoid ROGs (Weschler and Shields, 1999, 2003; Wainman et al., 2000; Sarwar et al., 2003; Destaillats et al., 2006; Sarwar and Corsi, 2007; Zuraimi et al., 2007; Coleman et al., 2008b; Waring et al., 2008; Chen and Hopke, 2009a, 2009b, 2010; Fadeyi et al., 2009; Chen et al., 2011; Waring et al., 2011).

In the absence of very strong indoor emissions of ROGs, the dominant loss mechanism of ozone is reactions on indoor

* Corresponding author. Tel.: +1 215 895 1502; fax: +1 215 895 1363.
E-mail address: msw59@drexel.edu (M.S. Waring).

1352-2310/$ – see front matter © 2013 Elsevier Ltd. All rights reserved.
http://dx.doi.org/10.1016/j.atmosenv.2013.11.009

surfaces (Weschler, 2000), which may be coated with a film of organic compounds that came from the surface or partitioned there from the gas phase (Liu et al., 2003; Weschler and Nazaroff, 2008). Ozone can react on surfaces with sorbed terpenoids (Fick et al., 2005; Shu and Morrison, 2011; Springs et al., 2011; Shu and Morrison, 2012), and Waring and Siegel (2013) showed that ozone reactions with sorbed D-limonene generated SOA meaningfully in chamber experiments. However, D-limonene is volatile so the SOA was formed by simultaneously occurring surface and gas phase reactions between ozone and D-limonene. This current work investigates this phenomenon further and explores whether SOA formation can be initiated entirely by ozone reactions with surface-sorbed squalene (2,6,10,15,19,23-hexamethyl-2,6,10,14,18,22-tetracosahexaene). Surface sorbed squalene is ubiquitous indoors; it is the most abundant ozone-reactive constituent of the human sebum (Nicolaides, 1974), so human skin is a significant ozone sink (Tamas et al., 2006; Weschler et al., 2007; Coleman et al., 2008a), and due to desquamation, it is a component of settled dust (Weschler et al., 2011).

Recent research on ozone reactions with sorbed squalene in chamber systems and with human skin in occupied spaces has determined that these reactions yield volatile and semivolatile compounds as both primary and secondary products, including acetone, 4-oxopentanal (4-OPA), 6-methyl-5-hepten-2-one (6-MHO), geranyl acetone, and various high molecular weight, polyunsaturated aldehydes (Fruekilde et al., 1998; Wells et al., 2008; Petrick and Dubowski, 2009; Wisthaler and Weschler, 2010). Some of these products could partition to form SOA mass; some could potentially even lead to nucleation of new particles. Related research has shown that gas phase reactions between ozone and squalene emitted by a laser printer may generate SOA (Wang et al., 2012). As such, we explored the SOA mass and number formation initiated by ozone and squalene surface reactions in steady state experiments, at varying ozone and relative humidity (RH) conditions, in the absence of any seed particles. Higher ozone mole fractions and air exchange rates than typical of indoors were used to emphasize the impacts of the surface reactions on SOA formation, allowing us to speculate on the underlying mechanism.

2. Methodology

2.1. Experimental apparatus

Experiments were performed in a continuously mixed flow reaction (CMFR) chamber system that consisted of air and ozone sources, the reaction chamber, and measurement instruments. The air source consisted of a zero air generator (Environics 7000), humidifier (Pyrex® washing bottle, 500 mL, filled with deionized water), ozone generator (2B Technologies model 306), mass flow controllers (Aarlborg GFC171S), and a temperature and relative humidity (RH) sensor (HOBO U14). The system was capable of providing clean air of a desired ozone mole fraction and RH into the chamber, at a flow rate of 3.35 L min^{-1}. The reaction chamber was a 37.1 L stainless steel chamber (Eagle Stainless CTH-36), so the air exchange rate was 5.42 h^{-1}, which was operated at this elevated state to emphasize surface reactions over gas phase reactions (Wang and Morrison, 2006). The same ozone monitor (2B Technologies model 205, 10 s intervals) was used to measure both inlet and outlet ozone concentrations using switching valves. A Scanning Electrical Mobility Sizer (SEMS) (BMI model 2002) was used for measuring SOA distributions within the particle diameter range of 10–900 nm, with a scan measured every 136 s.

2.2. Experimental protocol

Experiments were performed at RH of near 20% or 50% and at room temperature. The inlet ozone was varied across experiments so that the chamber ozone mole fraction ranged from 57 to 500 ppb. The initial squalene concentration was constant across experiments at 3.9×10^{16} molec cm^{-2} at an area of 255 cm^2, which was attained by dosing four Pyrex® petri dish bottoms with 3 mL each of a stock solution of 1.4×10^{-3} M squalene (Sigma Aldrich, 99% purity) in methanol (Sigma Aldrich, 99% purity). This squalene concentration approximates that on human skin (Youn et al., 2002). Before each experiment, the chamber was cleaned with 1000 ppb of ozone in the inlet air overnight. After the purging, the ozone was turned off and only clean air was introduced until the chamber ozone was zero. Then the chamber was opened and petri dish bottoms with the squalene/methanol solution were placed onto the chamber bottom. The chamber was flushed with clean air for another 1.5 h so that the methanol could evaporate. We assumed that negligible squalene evaporated due to its low vapor pressure (Wells et al., 2008). There were no measured particles or ozone in the chamber by the end of the flushing time.

After the 1.5 h purging time, ozone was introduced into the chamber. Experiments were run until ozone and chamber particles reached steady state. Particle and ozone data from the last hour of steady state were used in the data analysis as described in Section 2.3. The inlet ozone mole fraction was recorded at the end of the experiment for 20 min. Previous characterization experiments showed the ozone generator capable of producing steady mole fractions. The SOA number was converted to mass by assuming the particles were spherical with a unit density of 1 g cm^{-3}. The density of SOA due to squalene oxidation is unknown, and we report this 'normalized mass' so that an actual mass can be calculated in the future by multiplying our normalized mass by the actual density once it is known.

2.3. Parameterization of experimental results

We parameterized ozone reactions with chamber and squalene surfaces with the ozone deposition velocity, v_d (m h^{-1}), which is a mass transfer coefficient that relates ozone flux to a surface and the bulk air concentration (Cano-Ruiz et al., 1993). To do so, a mass balance on chamber ozone was written, which is Equation (1):

$$\frac{dC_{O_3}}{dt} = \lambda C_{O_3,inlet} - \left(\lambda + \frac{v_{d,w}(A_w - A_{sq})}{V} + \frac{v_{d,sq}A_{sq}}{V}\right)C_{O_3} \quad (1)$$

where λ (h^{-1}) is the air exchange rate; C_{O_3} and $C_{O_3,\,inlet}$ (ppb) are the ozone mole fractions in the chamber and the inlet flow, respectively; $v_{d,w}$ and $v_{d,sq}$ (m h^{-1}) are the deposition velocities to the stainless steel chamber walls and the squalene, respectively; A_w and A_{sq} (m^2) are the surface areas of the chamber walls and the squalene, respectively; and V (m^3) is the chamber volume. (The $A_w = 0.6$ m^2, and the A_{sq} and V are given in the previous subsection.) The left side of Equation (1) represents the time rate of change of ozone in the chamber; on the right side, the positive terms are sources of ozone and the negative terms are losses. The source of ozone is that contained in the inlet air, and losses of ozone are due to air exchange, reaction with the chamber walls, and reaction with the sorbed squalene.

Since experiments were analyzed at steady state, Equation (1) was set to zero and solved for $v_{d,sq}$, which is shown as Equation (2):

$$v_{d,sq} = \frac{\lambda V}{A_{sq}}\left(\frac{C_{O_3,inlet}}{C_{O_3}} - 1\right) - \frac{v_{d,w}(A_w - A_{sq})}{A_{sq}} \quad (2)$$

Equations (1) and (2) neglect reactions with ozone and desorbed ozone–squalene reaction products in the gas phase because volatile products were not measured. Though the short chamber residence time was chosen to reduce the impact of neglecting these reactions, we should note that our calculated $v_{d,sq}$ will be somewhat artificially inflated. All terms in Equation (2) were measured or known except $v_{d,w}$, which is a function of the chamber ozone mole fraction. Therefore, before any formation experiments, the $v_{d,w}$ was characterized with a prior set of experiments for only the empty stainless steel chamber at RH = 20% and 50% over a range of ozone mole fractions. Equation (1) was solved for $v_{d,w}$ at steady state with the term $A_{sq} = 0$ m^2. Power law functions were fit to these results, and the fits were $v_{d,w} = 0.13 \cdot C_{O_3}^{-0.56}$ ($R^2 = 0.81$) and $v_{d,w} = 0.071 \cdot C_{O_3}^{-0.66}$ ($R^2 = 0.98$), for RH = 20% and 50%, respectively.

SOA mass formation due to gas phase reactions is typically parameterized with the aerosol mass fraction (AMF or ξ), which is often called the SOA yield and is the ratio of the amount of SOA produced to the amount of the ROG consumed (Odum et al., 1996). However, for SOA from surface reactions it is more attractive mathematically to parameterize formation as the ratio of SOA produced to the amount of ozone reacted with the surface-sorbed molecules (Waring and Siegel, 2013), as with:

$$\xi_{O_3/sq,M} = \frac{\Delta C_{SOA,M}}{\Delta C_{O_3/sq,M}} \quad (3)$$

where $\xi_{O_3/sq,M}$ (−) is the surface reaction-initiated AMF that describes the change in the SOA mass concentration, $\Delta C_{SOA,M}$ (μg m^{-3}), that corresponds to a certain amount of ozone mass that reacted with squalene, $\Delta C_{O_3/sq,M}$ (μg m^{-3}). Similarly, we have defined an SOA aerosol number fraction (ANF) initiated by ozone reactions with surface-sorbed squalene, $\xi_{O3/sq,N}$ (# cm^{-3} per μg m^{-3}), so that:

$$\xi_{O_3/sq,N} = \frac{\Delta C_{SOA,N}}{\Delta C_{O_3/sq,M}} \quad (4)$$

where $\Delta C_{SOA,N}$ (# cm^{-3}) is the number concentration of SOA generated by a certain amount of ozone mass reacted with surface-sorbed squalene.

The ozone deposition velocity to the sorbed squalene may be combined with the surface AMF or ANF to describe the behavior of SOA mass and number, respectively, due to ozone–squalene reactions in the chamber. The mass balance for SOA is as shown in Equation (5):

$$\frac{dC_{SOA,M}}{dt} = \xi_{O_3/sq,M} C_{O_3,M} \frac{v_{d,sq} A_{sq}}{V} - (\lambda + \beta_{SOA,M}) C_{SOA,M} \quad (5)$$

where $C_{SOA,M}$ and $C_{O_3,M}$ (μg m^{-3}) are the chamber SOA and ozone mass concentrations, respectively; and $\beta_{SOA,M}$ (h^{-1}) is the loss rate of SOA mass to the chamber surfaces. The left side of Equation (5) represents the time rate of change of SOA mass; on the right side, the positive terms are sources of SOA mass and the negative terms are losses. The SOA source is that initiated by ozone reactions with sorbed squalene and losses are due to air exchange and deposition to the chamber walls. Though not shown, a number balance that is similar in form to Equation (5) may be written for chamber SOA number concentrations.

Equation 5 may be set to zero, solved at steady state, rearranged, and used with other measured or known parameters (e.g., $C_{SOA,M}$, $C_{O_3,M}$, λ, etc.) to calculate parameters that quantify and describe the SOA formation. We also want to explicitly note here that the surface AMF and ANF as we use them effectively describe the mass and number formation *initiated* by ozone–squalene reactions; subsequent gas phase reactions among ozone and any volatile products are taken into account as well. The surface AMF ($\xi_{O_3/sq,M}$) at steady state is Equation (6):

$$\xi_{O_3/sq,M} = \frac{V}{A_{sq} v_{d,sq}} \cdot \frac{(\lambda + \beta_{SOA}) C_{SOA,M}}{C_{O_3,M}} \quad (6)$$

The only unmeasured or unknown term in Equation (6) is $\beta_{SOA,M}$. Using the theory of Lai and Nazaroff (2000) with a density of 1 g cm^{-3} and friction velocity of 2.9 cm s^{-1} (determined by the deposition velocity theory of Cano-Ruiz et al. (1993) as mentioned in Section 3.2), an integrated $\beta_{SOA,M}$ was determined for each steady state mass distribution. To determine the surface ANF ($\xi_{O_3/sq,N}$), a similar procedure was used with a SOA number balance, including determining a separate integrated deposition rate for SOA number.

Secondary emission rates of SOA mass and number due to the ozone–squalene reactions, called the $SER_{SOA,M}$ (μg m^{-2} h^{-1}) and $SER_{SOA,N}$ (# cm^{-2} h), respectively, were also determined. The $SER_{SOA,M}$ is the SOA mass emission rate normalized by the squalene area, and at steady state is Equation (7):

$$SER_{SOA,M} = \frac{C_{SOA,M}(\lambda + \beta_{SOA,M})}{A_{sq}/V} = \xi_{O_3/sq,M} C_{O_3,M} v_{d,sq} \quad (7)$$

Yet again, a similar procedure was used to calculate the $SER_{SOA,N}$ with a SOA number balance. Also, since we use the 'normalized mass' in Equations (6) and (7), we actually report 'normalized AMFs' and 'normalized mass SERs' that can be multiplied by the actual density in the future.

3. Results and discussion

3.1. Summary of experimental conditions and behavior

Table 1 lists the conditions for the 13 experiments that measured SOA formation initiated by ozone reactions with surface-sorbed squalene, which are labeled Sq1–Sq13. Parameter uncertainty was calculated as the quadrature sum of the instrument accuracy and standard deviation during the steady state periods and propagated through relevant calculations. Six low RH experiments, Sq1–Sq6, had a mean (±uncertainty) RH of 21 (0.5)%; seven moderate RH experiments, Sq7–Sq13, had a mean of 51 (1)%; and the mean temperature over all experiments was 22 (1)°C. The steady state chamber ozone mole fractions ranged from 57 to 392 ppb for Sq1–Sq6 and from 60 to 500 ppb for Sq7–Sq13. Table 1 also lists the steady state deposition velocity of ozone to the sorbed squalene ($v_{d,sq}$), the steady state chamber SOA mass and number, and the unimodal lognormal fits (GM = geometric mean and GSD = geometric standard deviation) for the steady state SOA size distributions. The deposition rates for SOA mass and number ranged from 0.12 to 0.89 h^{-1} and 0.33 to 1.3 h^{-1}, respectively. Experiment Sq1 showed very little particle formation and is treated as an outlier and not included in our analysis.

Typical results are shown in Fig. 1, which displays the continuous chamber ozone mole fractions and SOA mass and number concentrations for experiments Sq2, Sq6, Sq8 and Sq13, which represent low and high ozone experiments at 21% and 51% RH, respectively. The chamber had an ozone loss rate of 9.32–12.4 h^{-1} (air exchange + ozone surface reaction rates) across all experiments, so ozone approached steady state within ~20 min of introduction. Due to these high loss rates, there is a reasonable chance that the unknown loss rate due to ozone gas phase reactions is not highly significant and the $v_{d,sq}$ are not artificially inflated to a large extent, but we cannot say this for certain. The ozone was steady or only slightly increased over time (i.e., changed by <2% per

Table 1
Means (±uncertainty or standard deviation, as noted) of steady state results from experiments measuring SOA formation initiated by ozone reactions with surface-sorbed squalene at different ozone and relative humidity conditions.

Exp[a]	Temp[b,f] (°C)	RH[c,f] (%)	Inlet ozone $C_{O_3,\ inlet}$[f] (ppb)	Ozone to squalene deposition velocity $v_{d,sq}$[f] (cm s^{-1})	Well-mixed chamber outlet			
					Ozone C_{O_3}[f] (ppb)	SOA mass[d] $C_{SOA,M}$[g] (μg m^{-3})	SOA number[e]	
							$C_{SOA,N}$[g] (# cm^{-3})	GM (nm)	GSD (−)
Sq1	22 (0.2)	22 (0.6)	125 (12)	0.25 (0.03)	57 (2.1)	2.5×10^{-5} (10^{-5})	3.6 (1.6)	19.9	1.34
Sq2	23 (0.2)	21 (0.5)	241 (6.3)	0.26 (0.01)	107 (3.0)	0.17 (0.02)	1891 (87.6)	40.7	1.63
Sq3	23 (0.2)	21 (0.5)	331 (7.5)	0.24 (0.008)	154 (3.4)	0.14 (0.01)	1914 (103)	38.3	1.63
Sq4	22 (0.2)	21 (0.5)	547 (13)	0.17 (0.006)	299 (6.4)	0.29 (0.02)	1755 (50.9)	46.6	1.69
Sq5	22 (0.2)	20 (0.5)	768 (17)	0.23 (0.007)	368 (7.6)	0.36 (0.02)	2144 (75.0)	48.0	1.71
Sq6	22 (0.2)	19 (0.5)	771 (19)	0.20 (0.007)	392 (8.1)	0.54 (0.02)	2342 (99.0)	52.7	1.75
Sq7	23 (0.2)	50 (1)	130 (4.3)	0.25 (0.01)	60 (1.9)	0.01 (6×10^{-4})	180.1 (24.2)	30.1	1.51
Sq8	23 (0.2)	52 (1)	275 (5.7)	0.15 (0.005)	160 (3.5)	0.05 (0.04)	343.7 (20.1)	39.5	1.62
Sq9	22 (0.2)	51 (1)	300 (6.3)	0.16 (0.005)	170 (4.2)	0.07 (0.02)	515.9 (17.3)	46.4	1.56
Sq10	23 (0.2)	49 (1)	567 (12)	0.15 (0.004)	332 (7.0)	0.61 (0.04)	2017 (82.1)	57.6	1.76
Sq11	23 (0.2)	51 (1)	700 (14)	0.15 (0.004)	408 (8.7)	1.4 (0.09)	2972 (80.1)	65.0	1.82
Sq12	22 (0.2)	49 (1)	754 (20)	0.17 (0.006)	414 (9.6)	2.2 (0.09)	5125 (292)	62.7	1.85
Sq13	23 (0.2)	52 (1)	877 (18)	0.16 (0.005)	500 (10)	4.2 (0.2)	5699 (193)	74.1	1.86

[a] Experiment label.
[b] Temperature.
[c] Relative humidity.
[d] Assuming a particle density of 1 g cm^{-3}.
[e] Unimodal lognormal fits were applied to the steady state particle size distributions; GM = geometric mean diameter; GSD = geometric standard deviation.
[f] Parameters in parentheses were overall uncertainties.
[g] Parameters in parentheses were one standard deviation of the mean at steady state.

hour for the highest case), indicating that the ozone–squalene reaction rate was nearly constant. The lowest ozone experiments required more time for SOA to approach a steady state condition (~7 h) than the highest ozone experiments (~2 h).

3.2. Ozone deposition to squalene and chamber surfaces

The $v_{d,sq}$ ranged from 0.15 to 0.27 cm s^{-1} overall experiments at steady state. Sorbed squalene is highly reactive (Wells et al., 2008), and using the theory of Cano-Ruiz et al. (1993), we estimated for the overall mean $v_{d,sq}$ = 0.2 cm s^{-1} that the total resistance of the ozone deposition to surface sorbed squalene was dominated by transport resistance (92.6% of total) rather than reaction resistance (7.4% of total), and that the friction velocity was 2.9 cm s^{-1} (this friction velocity was used in SOA deposition calculations as mentioned in Section 2.3). The ozone mole fraction had no impact on $v_{d,sq}$. However, the $v_{d,sq}$ was slightly higher at lower RH, and the means (±uncertainty) were 0.23 (0.03) and 0.17 (0.04) cm s^{-1} for RH = 21% and 51%, respectively; thus, the extra water vapor at higher RH may have competed with ozone–squalene reactions, as witnessed by Waring and Siegel (2013). These $v_{d,sq}$ are similar to those for ozone reactions with human occupants, which were 0.20–0.23 cm s^{-1} in a simulated aircraft cabin (Tamas et al., 2006) and 0.4–0.5 cm s^{-1} in an office (Wisthaler and Weschler, 2010). The reactions of ozone with squalene dominated those with the chamber walls, and $v_{d,w}$ ranged from 8.6×10^{-5} to 4.7×10^{-4} cm s^{-1} for Sq2–Sq6 with RH = 21% and $(0.25–3.3) \times 10^{-4}$ cm s^{-1} for Sq7–Sq13 with RH = 51%.

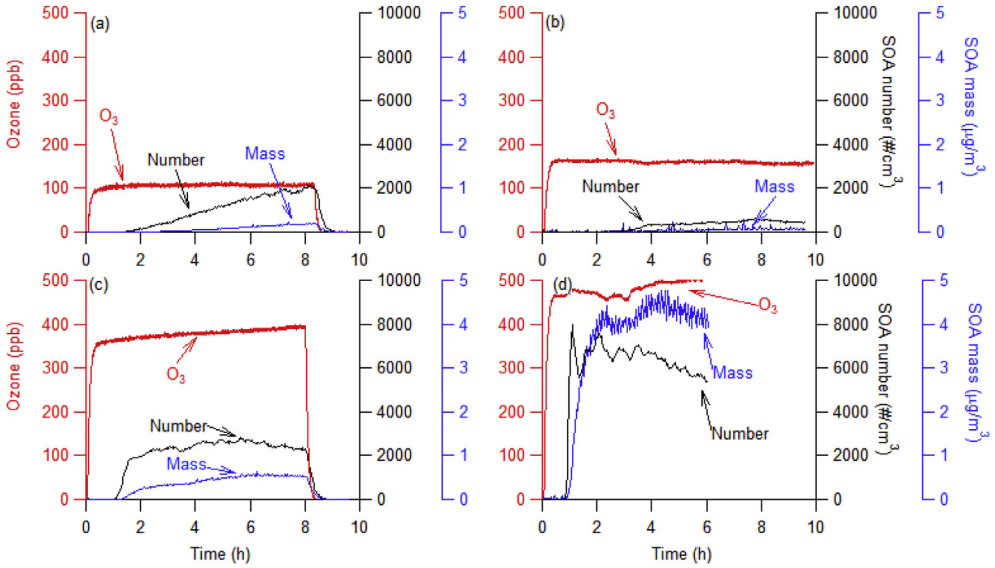

Fig. 1. Representative time series plots for chamber experiments exploring SOA formation initiated by surface reactions between ozone and sorbed squalene, for experiments (a) Sq2 and (c) Sq6, with a relative humidity (RH) of 21%, and (b) Sq8 and (d) Sq13, with RH of 51%. Time zero coincides with the introduction of ozone into the chamber.

3.3. SOA mass formation

Steady state SOA mass concentrations are listed in Table 1; also, the steady state SOA mass secondary emission rates ($SER_{SOA,M}$) and the surface AMFs ($\xi_{O_3/sq,M}$) are plotted versus the chamber ozone mole fraction in Fig. 2a and c, for each RH condition. For all but one exception in the RH = 21% condition (Sq2-Sq3), the mass concentrations and the SERs increased monotonically with increasing ozone, indicative of the higher rate of product formation due to ozone–squalene reactions at higher ozone mole fractions. Low mass concentrations were observed overall; this is certainly a function of our high chamber air exchange rate of 5.42 h^{-1}, which is higher than in typical buildings. However, one can use the $SER_{SOA,M}$ to explore the potential formation at other air exchange or loss rates by using a rearranged form of Equation (7) solving for $C_{SOA,M}$. For instance, if the air exchange rate were 0.5 h^{-1}, which is near the median air exchange rate for U.S. residences (Murray and Burmaster, 1995), all SOA concentrations listed in Table 1 would be a factor of 10.8 larger. We should point out that using the $SER_{SOA,M}$ in this way assumes an inverse relationship between the mass of SOA formed and the air exchange rate. This assumption is likely untrue because the $SER_{SOA,M}$ is a function of the surface AMF ($\xi_{O_3/sq,M}$), which may have different magnitudes at different air exchange rates (the dependence of AMFs on the air exchange rate has not yet been explored in the literature).

The surface AMFs were low in magnitude and ranged from near zero to ~0.006; these are much lower than the surface AMFs of 0.70–0.91 in Waring and Siegel (2013) for ozone/D-limonene reactions at chamber mole fractions of ~5 ppb of ozone and ~400–650 ppb of D-limonene. Of course, these surface AMFs cannot be directly compared, as they were determined at different air exchange rates and are for different reactant concentrations and reactants entirely, but they are still useful to compare to get a sense of scale. The surface AMFs increased exponentially with the ozone mole fractions for the RH = 51% experiments, but they were approximately constant over the RH = 21% experiments. At lower ozone mole fractions (< ~300 ppb), there were higher AMFs for the RH = 21% than RH = 51% condition, while at higher mole fractions (> ~300 ppb), this trend was reversed. This behavior is somewhat atypical as increases in gas phase AMFs and RH are usually concomitant (Jonsson et al., 2006). As will be discussed in Section 3.4, more nucleation occurred in the RH = 21% condition at these low ozone mole fractions than for the RH = 51% condition at low ozone, so this difference is likely due to that increased mass from the higher nucleation rates at low RH.

As an absorptive phenomenon, gas phase AMFs increase with the organic mass concentration (Odum et al., 1996); surface AMFs have not previously been investigated in this manner, as Waring and Siegel (2013) determined surface AMFs for ozone/D-limonene reactions within a narrow range of formed SOA mass concentrations. The mass formation in our experiments ranged orders of magnitude, so we plotted the surface AMF as a function of the chamber SOA mass concentration in Fig. 3. The surface AMFs increased with the SOA concentration for both RH conditions, though much more strongly for RH = 51%, so we have fit the surface AMF for RH = 51% as a function of the SOA mass concentration with Equation (8):

$$\xi_{O_3/sq,M} = \frac{\Delta C_{SOA,M}}{\Delta C_{O_3/sq,M}} = \sum_i \left(\frac{\alpha_{i,\ surface}}{1 + \left(c_i^* / C_{SOA,M} \right)} \right) \tag{8}$$

where the right-most side expresses the surface AMF as a multi-product model (Odum et al., 1996; Presto and Donahue, 2006); $\alpha_{i,surface}$ is the mass-based yield of product i initiated by surface reactions; and c_i^* (μg m^{-3}) is the effective gas phase saturation concentration of product i. Equation (8) is similar in form to that for the gas phase AMF, with the difference being that the gas phase AMF is the ratio of the mass of SOA formed to the mass of the ROG consumed. However, for a one-to-one molar ratio of ozone consumed and squalene reacted, Equation (8) should also be valid. It fits the data well, and using the 'volatility basis set' (VBS) with $c_i^* = \{0.001, 0.01, 0.1, 1, 10\}$, the $\alpha_{i,surface} = \{9.92 \times 10^{-7}, 1.31 \times 10^{-4}, 7.35 \times 10^{-5}, 9.90 \times 10^{-5}, 1.83 \times 10^{-2}\}$ for RH = 51%, using the fitting procedure in Stanier et al. (2008). The RH = 21% surface AMFs lie near the RH = 51% VBS curve.

3.4. SOA number formation

The steady state SOA number concentrations for each experiment are also in Table 1, and the steady state number secondary emission rates, $SER_{SOA,N}$, and the surface aerosol number fractions, ANF ($\xi_{O_3/sq,N}$), are plotted as a function of ozone mole fraction in Fig. 2b and d, for each RH condition. For RH = 21%, the number

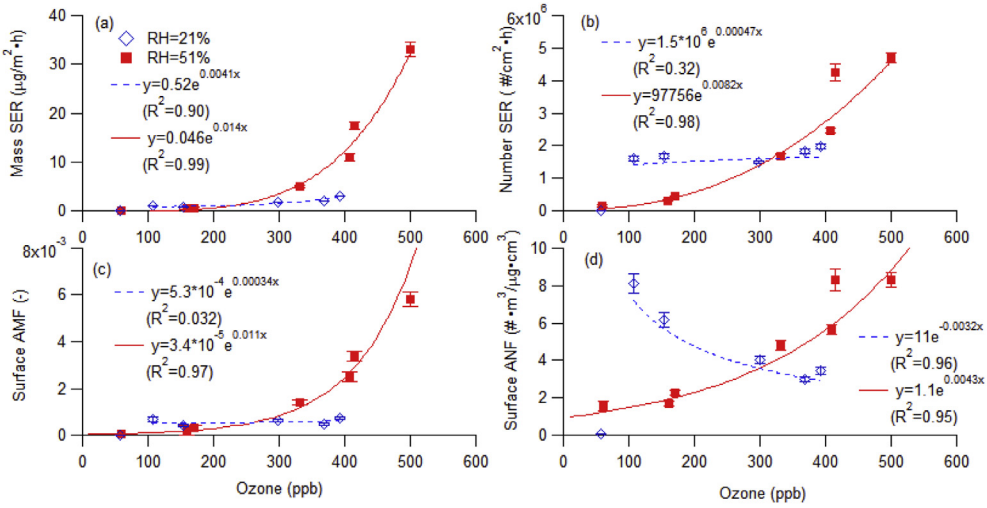

Fig. 2. Steady state (a) mass and (b) number secondary emission rates (SER), and surface (c) aerosol mass fractions (AMF) and (d) aerosol number fractions (ANF) for 13 ozone–squalene SOA formation experiments. Whiskers are uncertainties; exponential fits are provided (excluding Sq1).

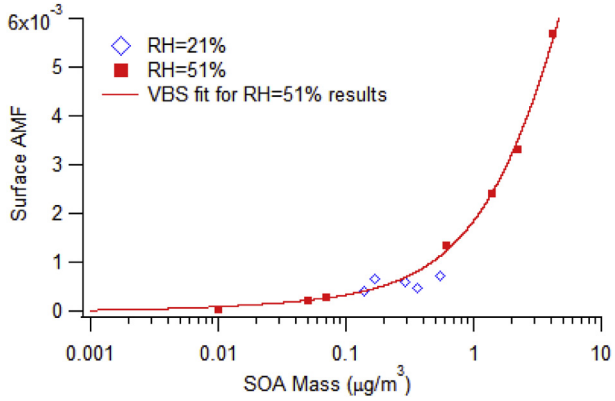

Fig. 3. Steady state aerosol mass fractions (AMF) as a function of SOA mass due to ozone–squalene surface reactions, for RH = 21 and 51%. An AMF curve was fit to the RH = 51% experiments using the 'volatility basis set' (see text for details and fit parameters). Experiment Sq1 is not included.

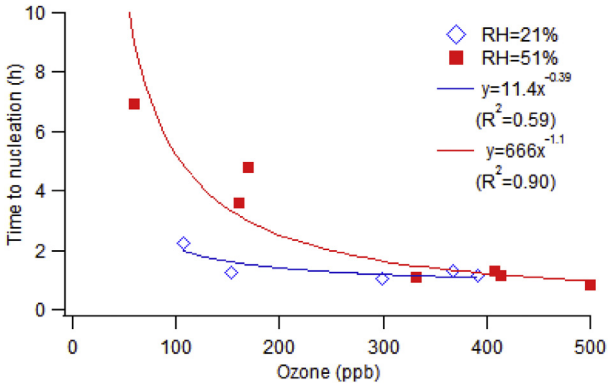

Fig. 4. Time to nucleation (using a concentration of at least 150 # cm^{-3} as the threshold) as a function of steady state ozone mole fractions for experiments measuring SOA formation initiated by surface reactions between ozone and squalene. Experiment Sq1 is not included.

formation results did not increase monotonically with ozone mole fractions. For experiments Sq2–Sq6, the steady state SOA number formation was similar and was 1755–2342 # cm^{-3}. Conversely, for the RH = 51% experiments Sq7–Sq13, the number concentration increased exponentially with the ozone mole fraction, and the range was larger at 180–5699 # cm^{-3}. As with mass formation, the number formation results might be higher for the same concentrations at lower air exchange rates. Finally, the GM and GSD for lognormal fits for the steady state size distributions are listed in Table 1. For all but two exceptions (Sq2-Sq3 and Sq11-Sq12), higher ozone (and thus more products) shifted the size distribution to larger median diameters and somewhat to larger GSDs.

For parameterizing number formation, there is not a framework with the ANF, as there is with the VBS for the AMF, to describe how the ANF depends on organic aerosol concentration descriptors (i.e., number, surface area, or mass). However, the ANF is useful to report because it demonstrates the impact of the ozone mole fraction and RH on the number formation strength. For RH = 21%, the largest surface ANFs were for Sq2 and Sq3 with lower ozone mole fractions, and the ANF decreased as the chamber ozone mole fraction increased, when Sq1 is excluded. In a different manner, the surface ANFs for RH = 51% increased exponentially with ozone. These results imply that the chemistry favors nucleation for low RH and low ozone conditions, but there are no studies to which we could directly compare these results. Bonn et al. (2002) studied the nucleation from the ozonolysis of terpenes, and for β-pinene, nucleation was stronger at lower RH. Of course, β-pinene cannot be directly compared to squalene; however, both are terpenoid compounds with C–C double bonds not contained within ring structures.

We plotted the time to nucleation for each experiment in Fig. 4, using the start time of ozone introduction as time zero and the SEMS scan time of a chamber concentration of at least 150 # cm^{-3} as the time at which nucleation effectively occurred. Nucleation times ranged from 50 min to 6.9 h, decreased with ozone, and followed power law functions. To reiterate, there were not any seed particles in the chamber, so all SOA was due to nucleation initiated by ozone–squalene reactions. Since the chamber residence time of 10.7 min was always shorter than the time to nucleation, products initially sorbed to the surface must have been involved in the nucleation. Desorption is typically first order with sorbed mass (Weschler and Nazaroff, 2008), so species involved in secondary reactions that promoted nucleation likely began desorbing at rates meaningful enough to affect nucleation once they reached a large enough surface concentration. Thus, the observed power law trend is logical since higher ozone mole fractions would generate product mass more quickly. Since the ozone–squalene reaction rate was nearly constant, over time the product desorption and SOA formation rates would become steady, as was observed.

3.5. Implications of results

Our experiments do not allow us to observe the mechanism underlying the SOA formation process due to ozone–squalene reactions, but we can speculate on it by using scaling analyses. Primary and secondary products from ozone–squalene reactions have been identified (Wells et al., 2008; Wisthaler and Weschler, 2010) and are listed in Table 2; products of OH oxidation have been excluded since these may only be meaningful at higher ozone mole fractions than in this work (Petrick and Dubowski, 2009). Using the EPIWIN Suite 4.1, we have estimated for these products their saturation vapor pressures, P_s (atm), octanol–air partition coefficients, K_{OA} (–), and gas phase reaction rate constants with ozone, k_{O_3} (ppb^{-1} h^{-1}). The K_{OA} of a product is proportional to its affinity to partition to the particle phase and form SOA mass, as well as being proportional to its affinity to remain bound to surface after the reaction. Using the k_{O_3}, we calculated the half-life, $t_{1/2}$ (min), of each product as it reacts with ozone in the gas phase for our range of chamber ozone mole fractions. The chamber residence time is 10.7 min, so products with $t_{1/2}$ much less than this time likely react away quickly and may not be present at high enough concentrations in the chamber to contribute to SOA formation.

The products likely to partition to the particle phase and contribute to SOA mass are therefore those with moderate values of K_{OA} and high $t_{1/2}$, such as geranyl acetone, 4-MOD, and 4-MON. Low volatility compounds such as C17-trienal, C22-tetraenal, and C27-pentaenal could also contribute, but their quite high K_{OA} also indicate that they may largely remain surface bound instead. However, particles in the boundary layer may enhance desorption rates of semivolatile compounds (Liu et al., 2012; Benning et al., 2013) and increase their overall flux from the surface, which would enhance formation. It is unclear which products contribute to nucleation; nucleating species have very low P_s (Bonn et al., 2002), so C17-trienal, C22-tetraenal, and C27-pentaenal may be involved, despite their high K_{OA} and affinity to remain surface bound. Future work should investigate the specific mechanisms of SOA mass and number formation initiated by surface reactions.

Squalene is present indoors both in settled dust (Weschler et al., 2011) and on human skin (Wisthaler and Weschler, 2010), and it is conceivable that over time, surface bound reaction products due to

Table 2
Primary and secondary products of ozone–squalene surface and gas phase reactions, with parameters describing their partitioning and reaction behavior in our experimental chamber system.

Ozone/squalene reaction products[a]	Saturation vapor pressure[b], log (P_s) (log (atm))	Octanol–air partition coefficient[b], log (K_{OA}) (–)	Rate constant with ozone[b] k_{O3} (ppb^{-1} h^{-1})	Gas phase reaction half life[c] $t_{1/2}$ (min)
Propan-2-one (acetone)	0.49	2.3		
6-Methyl-5-hepten-2-one (6-MHO)	−1.7	4.1	0.038	2.2–22
1,4-Butanedial (succinic dialdehyde)	−1.2	4.8		
4-Oxopentanal (4-OPA)	−1.4	4.9		
Ethanedial (glyoxal)	0.53	5.2		
6,10-Dimethylundeca-5,9-dien-2-one (geranyl acetone)	−3.5	5.8	0.077	1.1–11
4-Methyl-4-octene-1,8-dial (4-MOD)	−3.4	6.5	0.038	2.2–22
4-Methyl-8-oxo-4-nonenal (4-MON)	−3.5	6.5	0.038	2.2–22
5,9,13-Trimethyltetradeca-4,8,12-trienal (C17-trienal)	−5.3	7.4	0.12	0.72–7.2
4,9,13,17-Tetramethyl-octadeca-4,8,12, 16-tetraenal (C22-tetraenal)	−6.7	9.1	0.15	0.54–5.4
4,8,13,17,21-Pentamethyl-docosa-4,8,12, 16,20-Pentaenal (C27-pentaenal)	−8.1	10.7	0.19	0.43–4.3

[a] Products were not measured, but these have been identified either by Wells et al. (2008) or Wisthaler and Weschler (2010). Products from squalene reactions with hydroxyl radicals are not included.
[b] Parameters including P_s, K_{OA}, and k_{O_3} were calculated based on EPIWIN Suite 4.1.
[c] $t_{1/2}$ was determined for ozone mole fractions of 50–500 ppb, which was the approximate range in our experiments.

squalene oxidation could increase to concentrations that would be necessary to promote desorption and subsequent SOA mass or number formation. We must point out that ozone reactions with human skin can also reduce SOA formation in certain environments. Fadeyi et al. (2013) observed that SOA mass and number concentrations were less when 20 occupants were present than when not present, inside of a simulated office with constant emissions of ozone and D-limonene. Our experiments support that finding since the magnitude of formation due to ozone–squalene reactions is much smaller than that of ozone and D-limonene surface (Waring and Siegel, 2013) or gas phase reactions. If it is important indoors, the SOA formation from ozone–squalene reactions would likely only be important in the absence of high indoor gas phase terpenoid concentrations.

Given our high ozone mole fractions and air exchange rates, we cannot extrapolate our results to estimate the magnitude of SOA formation due to ozone–squalene reactions indoors. However, the SOA formation was *entirely* initiated by ozone–squalene surface reactions in our experiments, which highlights their potential importance indoors. Also, due to potentially low AMFs as implied by this study, it appears more likely that ozone–squalene reactions on indoor surfaces may contribute more to new particle formation and SOA number, rather than mass, concentrations. Similarly, Waring and Siegel (2013) demonstrated that ozone reactions with surface-sorbed D-limonene enhanced nucleation rates significantly. Finally, these reactions between ozone and squalene could also increase SOA concentrations in the breathing zone, as Rim et al. (2009) determined that reaction products in the breathing zone can be elevated above room levels due to ozone reactions with human skin as the thermal plume travels up the human body. Future work should also explore these possibilities.

4. Conclusions

We performed 13 steady state experiments to explore the SOA formation initiated by ozone surface reactions with sorbed squalene, at an air exchange rate of 5.42 h^{-1}, RH of 21% and 51%, and ozone mole fractions of 57–500 ppb. SOA formation was detected for all experiments except one, indicating reactions between ozone and surface sorbed squalene could initiate SOA formation. Surface AMFs and ANFs (as described in Section 2.3) were quantified. SOA mass concentrations increased with ozone, most notably for RH = 51%. Surface AMFs were low in magnitude, and an AMF curve as a function of the chamber organic aerosol concentration was fit to a RH = 51% results using the 'volatility basis set', as a function of the chamber SOA mass concentration. SOA number formation was stronger than mass, especially at low ozone and RH conditions, and we speculate that ozone–squalene reactions may impact number, rather than mass, concentrations indoors. We cannot extrapolate our findings to real indoor spaces because we conducted experiments at high air exchange rates to emphasize surface over gas phase reactions. More research is needed to investigate this phenomenon at typical indoor conditions.

Acknowledgments

We wish to thank the DeCarlo group at Drexel for the use of the SEMS in the work presented here. This work was funded by the National Science Foundation (Award #1055584) and performed in the Drexel Air Resources Research Laboratory (DARRL), jointly run by Drs. Waring and DeCarlo.

References

Benning, J.L., Liu, Z., Tiwari, A., Little, J.C., Marr, L.C., 2013. Characterizing gas-particle interactions of phthalate plasticizer emitted from vinyl flooring. Environ. Sci. Technol. 47, 2696–2703.
Bonn, B., Schuster, G., Moortgat, G.K., 2002. Influence of water vapor on the process of new particle formation during monoterpene ozonolysis. J. Phys. Chem. A 106, 2869–2881.
Cano-Ruiz, J.A., Kong, D., Balas, R.B., Nazaroff, W.W., 1993. Removal of reactive gases at indoor surfaces: combining mass transport and surface kinetics. Atmos. Environ. 27A, 2039–2050.
Chen, X., Hopke, P.K., 2009a. A chamber study of secondary organic aerosol formation by linalool ozonolysis. Atmos. Environ. 43, 3935–3940.
Chen, X., Hopke, P.K., 2009b. Secondary organic aerosol from alpha-pinene ozonolysis in dynamic chamber system. Indoor Air 19, 335–345.
Chen, X., Hopke, P.K., 2010. A chamber study of secondary organic aerosol formation by limonene ozonolysis. Indoor Air 20, 320–328.
Chen, X., Hopke, P.K., Carter, W.P.L., 2011. Secondary organic aerosol from ozonolysis of biogenic volatile organic compounds: chamber studies of particle and reactive oxygen species formation. Environ. Sci. Technol. 45, 276–282.
Coleman, B.K., Destaillats, H., Hodgson, A.T., Nazaroff, W.W., 2008a. Ozone consumption and volatile byproduct formation from surface reactions with aircraft cabin materials and clothing fabrics. Atmos. Environ. 42, 642–654.
Coleman, B.K., Lunden, M.M., Destaillats, H., Nazaroff, W.W., 2008b. Secondary organic aerosol from ozone-initiated reactions with terpene-rich household products. Atmos. Environ. 42, 8234–8245.
Destaillats, H., Lunden, M.M., Singer, B.C., Coleman, B.K., Hodgson, A.T., Weschler, C.J., Nazaroff, W.W., 2006. Indoor secondary pollutants from

household product emissions in the presence of ozone: a bench-scale chamber study. Environ. Sci. Technol. 40, 4421–4428.
Fadeyi, M.O., Weschler, C.J., Tham, K.W., 2009. The impact of recirculation, ventilation and filters on secondary organic aerosols generated by indoor chemistry. Atmos. Environ. 43, 3538–3547.
Fadeyi, M.O., Weschler, C.J., Tham, K.W., Wu, W.Y., Sultan, Z.M., 2013. Impact of human presence on secondary organic aerosols derived from ozone-initiated chemistry in a simulated office environment. Environ. Sci. Technol. 47, 3933–3941.
Fick, J., Pommer, L., Åstrand, A., Östin, R., Nilsson, C., Andersson, B., 2005. Ozonolysis of monoterpenes in mechanical ventilation systems. Atmos. Environ. 39, 6315–6325.
Fruekilde, P., Hjorth, J., Jensen, N.R., Kotzias, D., Larsen, B., 1998. Ozonolysis at vegetation surfaces: a source of acetone, 4-oxopentanal, 6-methyl-5-hepten-2-one, and geranyl acetone in the troposphere. Atmos. Environ. 32, 1893–1902.
Jonsson, Å.M., Hallquist, M., Ljungström, E., 2006. Impact of humidity on the ozone initiated oxidation of limonene, d3-carene, and a-pinene. Environ. Sci. Technol. 40, 188–194.
Klepeis, N.E., Nelson, W.C., Ott, W.R., Robinson, J.P., Tsang, A.M., Switzer, P., Behar, J.V., Hern, S.C., Engelmann, W.H., 2001. The National Human Activity Pattern Survey (NHAPS): a resource for assessing exposure to environmental pollutants. J. Expo. Anal. Environ. Epidemiol. 11, 231–252.
Kroll, J.H., Seinfeld, J.H., 2008. Chemistry of secondary organic aerosol: formation and evolution of low-volatility organics in the atmosphere. Atmos. Environ. 42, 3593–3624.
Lai, A.C.K., Nazaroff, W.W., 2000. Modeling indoor particle deposition from turbulent flow onto smooth surfaces. J. Aerosol Sci. 31, 463–476.
Lee, S.C., Lam, S., Fai, H.K., 2001. Characterization of VOCs, ozone, and PM10 emissions from office equipment in an environmental chamber. Build. Environ. 36, 837–842.
Liu, C., Morrison, G.C., Zhang, Y., 2012. Role of aerosols in enhancing SVOC flux between air and indoor surfaces and its influence on exposure. Atmos. Environ. 55, 347–356.
Liu, Q.-T., Chen, R., McCarry, B.E., Diamond, M.L., Bahavar, B., 2003. Characterization of polar organic compounds in the organic film on indoor and outdoor glass windows. Environ. Sci. Technol. 37, 2340–2349.
Murray, D.M., Burmaster, D.E., 1995. Residential air exchange rates in the United States: empirical and estimated parametric distributions by season and climatic region. Risk Anal. 15, 459–465.
Nazaroff, W.W., Weschler, C.J., 2004. Cleaning products and air fresheners: exposure to primary and secondary air pollutants. Atmos. Environ. 38, 2841–2865.
Nicolaides, N., 1974. Skin lipids: their biochemical uniqueness. Science 186, 19–26.
Odum, J.R., Hoffmann, T., Bowman, F., Collins, D., Flagan, R.C., Seinfeld, J.H., 1996. Gas/particle partitioning and secondary organic aerosol yields. Environ. Sci. Technol. 30, 2580–2585.
Petrick, L., Dubowski, Y., 2009. Heterogeneous oxidation of squalene film by ozone under various indoor conditions. Indoor Air 19, 381–391.
Presto, A.A., Donahue, N.M., 2006. Investigation of a-pinene + ozone secondary organic aerosol formation at low total aerosol mass. Environ. Sci. Technol. 40, 3536–3543.
Rim, D., Novoselec, A., Morrison, G., 2009. The influence of chemical interactions at the human surface on breathing zone levels of reactants and products. Indoor Air 19, 324–334.
Sarwar, G., Corsi, R., 2007. The effects of ozone/limonene reactions on indoor secondary organic aerosols. Atmos. Environ. 41, 959–973.
Sarwar, G., Corsi, R., Allen, D., Weschler, C., 2003. The significance of secondary organic aerosol formation and growth in buildings: experimental and computational evidence. Atmos. Environ. 37, 1365–1381.
Shu, S., Morrison, G.C., 2011. Surface reaction rate and probability of ozone and alpha-terpineol on glass, polyvinyl chloride, and latex paint surfaces. Environ. Sci. Technol. 45, 4285–4292.
Shu, S., Morrison, G.C., 2012. Rate and reaction probability of the surface reaction between ozone and dihydromyrcenol measured in a bench scale reactor and a room-sized chamber. Atmos. Environ. 47, 421–427.
Singer, B.C., Destaillats, H., Hodgson, A.T., Nazaroff, W.W., 2006. Cleaning products and air fresheners: emissions and resulting concentrations of glycol ethers and terpenoids. Indoor Air 16, 179–191.
Springs, M., Wells, J.R., Morrison, G.C., 2011. Reaction rates of ozone and terpenes adsorbed to model indoor surfaces. Indoor Air 21, 319–327.
Stanier, C.O., Donahue, N., Pandis, S.N., 2008. Parameterization of secondary organic aerosol mass fractions from smog chamber data. Atmos. Environ. 42, 2276–2299.
Tamas, G., Weschler, C., Bakobiro, Z., Wyon, D., Stromtejsen, P., 2006. Factors affecting ozone removal rates in a simulated aircraft cabin environment. Atmos. Environ. 40, 6122–6133.
Wainman, T., Zhang, J.F., Weschler, C.J., Lioy, P.J., 2000. Ozone and limonene in indoor air: a source of submicron particle exposure. Environ. Health Perspect. 108, 1139–1145.
Wang, H., He, C., Morawska, L., McGarry, P., Johnson, G., 2012. Ozone-initiated particle formation, particle aging, and precursors in a laser printer. Environ. Sci. Technol. 46, 704–712.
Wang, H., Morrison, G.C., 2006. Ozone-initiated secondary emission rates of aldehydes from indoor surfaces in four homes. Environ. Sci. Technol. 40, 5263–5268.
Waring, M.S., Siegel, J.A., 2011. The effect of an ion generator on indoor air quality in a residential room. Indoor Air 21, 267–276.
Waring, M.S., Siegel, J.A., 2013. Indoor secondary organic aerosol formation initiated from reactions between ozone and surface-sorbed d-limonene. Environ. Sci. Technol. 47, 6341–6348.
Waring, M.S., Siegel, J.A., Corsi, R.L., 2008. Ultrafine particle removal and generation by portable air cleaners. Atmos. Environ. 42, 5003–5014.
Waring, M.S., Wells, J.R., Siegel, J.A., 2011. Secondary organic aerosol formation from ozone reactions with single terpenoids and terpenoid mixtures. Atmos. Environ. 45, 4235–4242.
Wells, J.R., Morrison, G.C., Coleman, B.K., 2008. Kinetics and reaction products of ozone and surface-bound squalene. J. ASTM Int. 5.
Weschler, C.J., 2000. Ozone in indoor environments: concentration and chemistry. Indoor Air 10, 269–288.
Weschler, C.J., Langer, S., Fischer, A., Beko, G., Toftum, J., Clausen, G., 2011. Squalene and cholesterol in dust from Danish homes and daycare centers. Environ. Sci. Technol. 45, 3872–3879.
Weschler, C.J., Nazaroff, W.W., 2008. Semivolatile organic compounds in indoor environments. Atmos. Environ. 42, 9018–9040.
Weschler, C.J., Shields, H.C., 1999. Indoor ozone/terpene reactions as a source of indoor particles. Atmos. Environ. 33, 2301–2312.
Weschler, C.J., Shields, H.C., 2003. Experiments probing the influence of air exchange rates on secondary organic aerosols derived from indoor chemistry. Atmos. Environ. 37, 5621–5631.
Weschler, C.J., Wisthaler, A., Cowlin, S., Tamas, G., Hodgson, A.T., Destaillats, H., Herrington, J., Zhang, J., Nazaroff, W.W., 2007. Ozone-initiated chemistry in an occupied simulated aircraft cabin. Environ. Sci. Technol. 41, 6177–6184.
Wisthaler, A., Weschler, C.J., 2010. Reactions of ozone with human skin lipids: sources of carbonyls, dicarbonyls, and hydroxycarbonyls in indoor air. Proc. Natl. Acad. Sci. U. S. A. 107, 6568–6575.
Youn, S.W., Kim, S.J., Hwang, I.A., Park, K.C., 2002. Evaluation of facial skin type by sebum secretion: discrepancies between subjective descriptions and sebum secretion. Skin Res. Technol. 8, 168–172.
Zuraimi, M.S., Weschler, C.J., Tham, K.W., Fadeyi, M.O., 2007. The impact of building recirculation rates on secondary organic aerosols generated by indoor chemistry. Atmos. Environ. 41, 5213–5223.